
Scalable Computing: Practice and Experience, ISSN 1895-1767, http://www.scpe.org
© 2024 SCPE. Volume 25, Issues 5, pp. 3427–3439, DOI 10.12694/scpe.v25i5.3162

# BRAIN TUMOR CLASSIFICATION USING REGION-BASED CNN WITH CHICKEN SWARM OPTIMIZATION

A SRAVANTHI PEDDINTI *, SUMAN MALOJI †, AND KASIPRASAD MANNEPALLI ‡

**Abstract.** Diagnosing and segmenting brain tumors manually through MRI imaging is a complex and time-consuming process. However, advancements in machine learning (ML) and deep learning (DL) technologies have enabled the automatic identification and categorization of brain tumors using computer-aided design. This study utilizes MRI data to develop a system for the automatic identification and categorization of brain tumors based on region-based convolutional neural networks (R-CNN). The proposed R-CNN approach, coupled with Chicken Swarm Optimization (CSO) technique, enables the identification and classification of brain tumors into stages. This method involves processing, segmenting, extracting features, and organizing the MRI images. Image preparation includes adaptive fuzzy filtering (AFF) to eliminate noise and enhance the quality of MRI images. To detect regions of brain injury, MRI scans undergo cranial segmentation and classification (CSO) based on Tsallis entropy-based image segmentation. A Residual Network (ResNet) is employed to fuse handcrafted and deep features, generating a meaningful set of feature vectors. Extensive simulations are conducted on the BRATS 2015 dataset to evaluate the improved performance in classifying brain tumors. The RCNN-CSO method demonstrates superior performance compared to other contemporary techniques, achieving a precision of 92.35%, sensitivity of 93.52%, specificity of 94.52 % and an accuracy of 96 % . This represents a significant improvement in brain tumor classification and its outomst accuracy.

**Key words:** Gliomas; Chicken swarm optimization; adaptive fuzzy filtering; RCNN-CSO; Residual network.

**1. Inntroduction.** Brain tumors, often called lesions or neoplasms, result from the uncontrolled proliferation of aberrant brain tissue. Brain tumors hurt brain function and threaten human life when abnormal tissue growth occurs in the brain. Physicians benefit from the use of computer-aided diagnosis systems that aid in the interpretation of medical images. It means that X-ray [1], ultrasound, and magnetic resonance imaging diagnostics must be dealt with by radiologists or specialists who must quickly review and analyze them to get clearance. With the emergence of machine learning algorithms and whole-side imaging, digital pathology has been approaching. Artificial Intelligence, pathological and radiological image processing, and CAD technology are merged into computer vision elements. It's becoming increasingly common for doctors to employ imaging techniques like MRIs and CT scans to identify cancers to better understand and treat patients. The non-invasive digital imaging techniques include CT scans, MRIs, X-rays, SPECTs, PETs, and ultrasounds. Machine Learning (ML) techniques can be used to improve early identification of brain cancers. Figure 1.1 depicts MRI images of the brain with a tumor and without a tumor.

The CSO algorithm is a variant of swarm intelligence optimization, initially proposed by Vasantharaj et al. [2] and further refined by Meng et al. [3]. The chicken flock's fitness ratings consider when the algorithm determines how to partition a flock of chickens into the three distinct categories of roosters, hens, and chicks. After that, each conducts their search in the solution space. Each particle in the algorithm indicates a different approach that could be taken to solve the issue. In the final step, a detailed comparison of the three groups' fitness values is performed to identify the globally ideal particle and the globally optimal value. The individuals with the highest overall fitness levels are designated as roosters among the flock. They can locate food across a greater area. The contributions of proposed RCNN-CSO for classifying the brain tumors:

- Deep learning algorithms use a revolutionary concept known as prediction at the pixel level.

*Department of ECE, Koneru Lakshmaiah Education Foundation, KLEF (Deemed to be University), Vaddeswaram, AP, India (sravanthi.angara@gmail.com).

†Department of ECE, Koneru Lakshmaiah Education Foundation, KLEF (Deemed to be University), Vaddeswaram, AP, India (Suman.maloji@kluniversity.in).

‡Department of ECE, Koneru Lakshmaiah Education Foundation, KLEF (Deemed to be University), Vaddeswaram, AP, India (mkasiprasad@kluniversity.in).

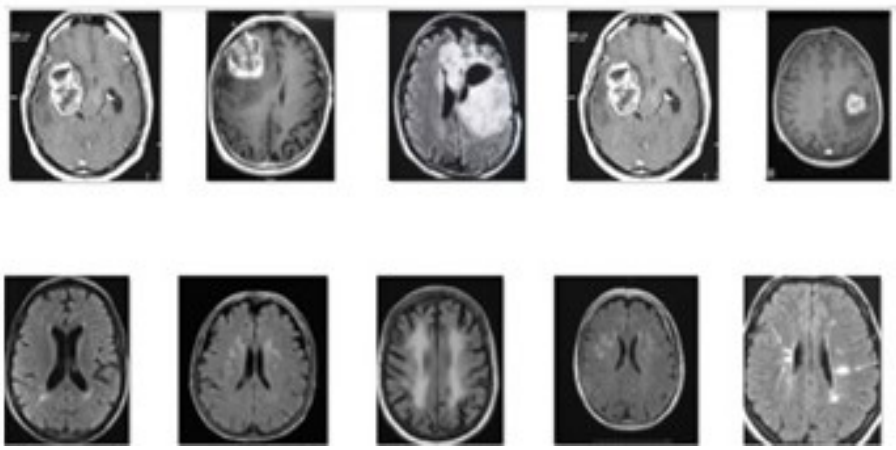

Fig. 1.1: Brain Tumor low intensity images.

- This study utilized a deep Convolutional Neural Network (CNN) known as RCNN-CSO to enhance the output process. Specifically, CNN was trained using MRI scans to classify brain tumors accurately.
- Pre-processing images with adaptive fuzzy filtering (AFF) removes noise and improves the quality of MRI images.
- MRI images are segmented using a technique called chicken swarm optimization (CSO), which uses Brain injury can be localized using Tsallis entropy-based picture segmentation.

The remaining sections are as follows: a discussion of relevant literature in Section 2, a presentation of the suggested method in Section 3, a display of results and discussions in Section 4, a performance validation in Section 5, and finally, a summary and conclusion in Section 6.

**2. Related Works.** The existing MRI-based brain tumor segmentation [4] approaches are divided into three groups: traditional techniques, classification strategies, cluster analysis, and deformable model methods. Demirhan et al. [5] classified brain MR images as tumors, white matter, grey matter, CSF, and edema. Since tumor growth on healthy brain tissues was studied, healthy and malignant brain tissues identifies. This information is crucial for treatment planning. Twenty glial tumor patients were examined using T1, T2, and FLAIR images.

In another study, Srinivas and Sasibhusana Rao [6] used K-means & Fuzzy C-means clustering for tumor detection in MRI scans. K-means and FCM clustering algorithms were compared using relative area, PSNR, segmented area, and MSE. Particle Swarm Optimization- With PSO, finding the best answer is more accessible, while Genetic Algorithms (GAs) get a near-optimal but not exact answer. Combining GAs and PSO determined the optimal degree of attraction. Combining The k-means & fuzzy c-means algorithms improved the precision with which tumor stages & sizes were determined. This method allows accurate and repeatable tumor tissue segmentation, like manual segmentation. It accelerates segmentation.

Abhishek Bal et al. [7] developed an automated method for segmenting brain tumors (RFCM). Using fuzzy membership and A rough set with a high and low bounce, rough-fuzzy C-means can address overlapping division. Both hard lower estimation and the fuzzy border have been helpful for RFCM brain tumor segmentation. C-means algorithm initial centroids may need to be revised. This work was used to speed up RFCM execution by picking starting centroids. Manocha et al. [8] mapped the tumor using automated segmentation in a different study. Brodmann area identification was included in the GUI technique for brain tumor segmentation. The research used 15 patients' T2-weighted images. Based on ethnicity, gender, and age, these data were divided into three groups. The "fuzzy" C indicates tumor clustering. Normalizing tumor segmentation data reduces image artifacts. This project's main benefit was a simple, user-friendly GUI simplifying the entire procedure.

Shree et al. [9] system for detecting, segmenting, & identifying neoplasms in the brain took time and effort.

Seeing abnormal brain tissue is difficult. Radiologists can't do further research using current procedures due to a lack of information on tumor grades. Justyna Tomicka J et al. [10] have proposed MRI modalities like The fields of Magnetic Resonance Spectroscopy (MRS), Diffusion Tensor Imaging (DTI), and Perfusion Imaging (PI) are gaining ground in the field of brain tumor segmentation. These methods have been used to localize tumors in the brain successfully. Kumar et al. [11] first proposed using optimization-driven deep convolutional neural networks to classify brain tumors. The MRI scans used for the analysis came from both the BRATS database and the Sim BRATS.

Rammurthy et al. [13] introduced the hybrid Whale Harris Hawks optimization (WHHO) for diagnosing tumors in the brain by exploiting MR imageries. The DCNN method was contemplated for the identification of tumors. The classification along segmentation method has been presented by Deb et al. [14] as a method for identifying malignant growths in the brain. Images' abnormality or normalcy establishes using a frog-leap-optimized Adaptive fuzzy deep neural network. Yin et al. [15] have shared their research in diagnosing brain tumors at an early stage. Here, early detection consists of 3 steps: reducing the noise in the background, extracting relevant features, and classifying them using a multi-layer perceptron NN. Using a deep neural network, Sultan et al. [16] demonstrated multi-classification of images of brain tumors. In this instance, they used a Deep Learning (DL) model and a convolutional neural network (CNN) to assign categories to the photographs.

Pandiselvi et al. [15] suggested an ACRC method for adaptable convex region contour. The normality or abnormality of this case was determined by using a Support Vector Machine (SVM) to slice categorization. Deepak et al. [17] employed a combination of convolutional neural networks and support vector machines. Brain tumor MRI data is automatically classified. In this study, classification was accomplished by using a computer-aided diagnostic (CAD) method for the human brain. CNN was utilized to extract the features. In addition to that, an SVM classifier uses to categorize the characteristics.

To classify brain tumors using MRI scans, Narmatha et al. [18] describe a hybrid fuzzy brain-storm optimization technique. The fuzzy brain-storm optimization algorithm is used to maximize the undefined parameters' effectiveness (FBSO). From the above discussion, we observed that the limitations in finding the usual medical imaging dataset for an analysis of a method can be complex. Therefore, many approaches test on a few data sets with varying metrics. Because of these challenges, comparisons between the presented methods and manually segmented medical images cannot be straightforward. Neural networks, clustering techniques like K-means and FCM, support vector machines, and deep learning algorithms like CNN can help enhance MRI picture quality by isolating the brain tumor. [19].

**3. Proposed Methodology.** This approach includes training a model built of numerous neural network processing layers. Creation of an automated Using MRI scan images, we present a deep learning-based method for tumor detection and classification in the brain. The stages of a brain tumor's development can identify and categorized using the RCNN-CSO method that has been proposed. Before the MRI scans can be processed to reduce noise and enhance the image quality, they must be pre-processed with AFF (Adaptive Fuzzy Filtering). MRI images are segmented using chicken swarm optimization (CSO), which uses picture segmentation using entropy to identify damaged brain sections. As can be seen in Figure 3.1, a valuable set of feature vectors are generated by employing a Residual Network (ResNet) to fuse both handcrafted and deep features.

**3.1. Chicken Swarm Optimization (CSO).** By utilizing the fractional-CSO algorithm, this paper presents a unique tumor classification methodology that is more accurate than existing methods. According to [20, 21], CSO is a single-objective optimization technique with biological impacts. It imitates how a flock of hens behaves hierarchically while hunting for food, with each chicken standing in for a potential optimization solution. CSO defines four guidelines for the perfect chicken behavior:

- A dominant rooster, hens, and chicks are present in every chicken swarm group.
- The fitness of each chicken determines whether it belongs to a group of hens, roosters, or chicks. The group is led by the roosters, which are the fittest chickens. A chick is a lesser chicken. Some are hens.
- Every G step, mother-child connections, dominance, and hierarchical relationships should shift.
- For nourishment, chickens follow their rooster. We expect that chickens will steal food from one another. Near their moms, chicks go foraging. The rooster wins the food fight. We distinguish between the following numbers in a swarm of N chickens: There are a total of RN roosters, HN hens, CN chicks,

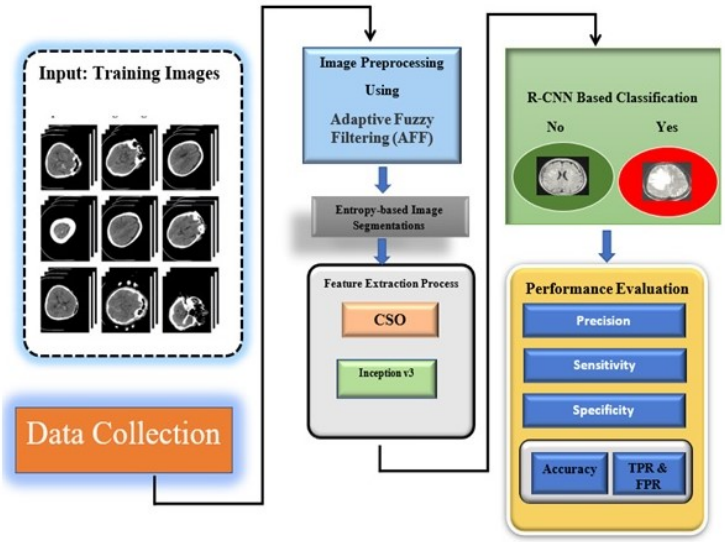


Fig. 3.1: RCNN - Methods for Detecting and Classifying Brain Tumors.

and MN mother hens. The xij coordinates of each chicken (I [1,..N], j [1,.D]) describe their location in D-dimensional space. Chickens come in three different varieties in CSO. Each species has its distinctive dance.

**3.2. Rooster Movement.** The roosters with the best fitness ratings can find food in more locations than those with lower fitness ratings. Eqs. (1) and (2) describe their motion.

$$x_{ij}^{t+1} = x_{ij}^{t} * \left(1 + Randn\left(0, \sigma^2\right)\right) \tag{3.1}$$

In this context, k is an arbitrary rooster index, and Randn (0, 2) is a zero-mean Gaussian distribution. A minor constant, 2, and the rooster's fitness, fi, are denoted below.

*Hen movement.* Hens engage in foraging behavior in the presence of another group member. In addition, they would strategically appropriate the high-quality food provided by their bird counterparts, all the while being constrained by their fellow gallinaceous companions. The more dominating chickens would triumph over obedient hens in a food fight. The equations (3.1) – (3.5) can be used to mathematically explain the movement of elements.

$$x_{ij}^{t+1} = x_{ij}^{t} * \left(S_1 + Randn * \left(x_{n,i}^{t} - x_{n,i}^{t}\right) + S_2 + Randn * \left(x_{n,i}^{t} - x_{n,i}^{t}\right)\right) \tag{3.2}$$

$$S_1 = exp\left(\frac{f_k - f_{r1}}{|f_{r2} + f_1|}\right) \tag{3.3}$$

$$S_2 = |f_{r2}| + f_1 \tag{3.4}$$

The variable Randn represents a random number that follows a uniform distribution between 0 and 1. While r2 is an index of a chicken, The variable r1 represents an index that relates to the rooster, explicitly referring to the groupmate of the I-th hen. (rooster or hen). It gets picked at random from the swarm (r1, r2).

*Chick movement.* Young chicks perform exploratory behaviors to find sustenance, often venturing away from their maternal figure. The movement of the chick is defined by Equation (3.6).

$$x_{ij}^{t+1} = x_{ij}^{t} + FL * \left(x_{m,j}^{t} - x_{ij}^{t}\right) \tag{3.5}$$

where x_(m,j)t, The position of the mother of the i-th chick, denoted as m, is defined within the range of 1 to N. FL, a parameter that quantifies the extent to which a chick will mimic the speed of its mother. To examine the distinctions among the several chicks, a random selection is made for the variable FL within the interval [0,2].

**3.3. Pre-Processing of Brain Tumor Images.** Tumor classification begins with pre-processing because making the subsequent procedure more realistic is crucial. We use the brain imaging dataset to obtain the input image of the brain. During the pre-processing stage, significant tumor sites are extracted [22]. Consider the database E of brain images, which it denotes as, and contains Bn images with [Q X R] dimensions.

$$F = \{C1, C2, \cdots\cdots\cdots Ci \cdots\cdots Cn\}; [Q \times R] \tag{3.6}$$

Cn represents the data set containing a cumulative count of brain images, denoted as the total number. In contrast, variable F indicates the database's specific quantity of brain photographs. In this scenario, the pre-processing function uses the image Bi from the database. Cropping the regions of interest from image Ci results in an image designated as C I with the dimension [Q R], which is the output of the pre-processing phase.C I = b1, b2,... bj,... bP the pre-processed image C I is characterised by its M number of pixels.

$$max_R \sum_{K=1}^{Q} b_j \left(X_c \left(R\right)\right) \tag{3.7}$$

where bj(Xc,(R)) The passage discusses an objective function that is specifically associated with the Kth feature of the data, denoted by (R). The standard parameter.

$$max_{x,R} \sum_{K=1}^{Q} w_j, b_j \left(X_c \left(R\right)\right) \tag{3.8}$$

the pixel values being represented by wj. To help with clustering model regularization, the expression of the sparse FCM is presented in eq 3.7 to 3.9.

$$maxH\left(X, R, g\right) = g^m \lambda \left(R\right) \tag{3.9}$$

**3.4. Feature extraction for brain tumor classification.** The segmented image C*kl is subsequently transmitted to the feature extraction stage, where the most salient characteristics are extracted from the segmented outcomes. Using feature extraction, we may simplify brain MRIs by eliminating unnecessary data. The mean value of the pixels is represented, which is shown in eq 3.10 to 3.13.

$$g_1 = \frac{1}{Q} \sum_{k=1}^{Q} C_{kq}^{*} \tag{3.10}$$

where $C_{jq}$ denotes the qth picture element of the image $C_j$ segmentation variance The dimension of feature f2 is determined by its mean value of [2 × 1]

$$g_2 = \left(\frac{1}{Q} \sum_{k=1}^{Q} \sqrt{C_{kq}^{*}}\right)^2 \tag{3.11}$$

Entropy is used to determine which pixels contain the most information.

$$g_3 = -\sum_{k=1}^{Q \sum_{kq}^{*}} C_{kq}^{*} log \tag{3.12}$$

The coverage feature determines the tumor region by calculating the total number of pixel positions and segmented points. The term "coverage" refers to the method used to determine the width and length of a tumor. On the other hand, the coverage characteristics of dimension [2x1] are stated as,

$$g_4 = \sum_{k=1}^{Q} \frac{w_j}{C^*_{kq}} \tag{3.13}$$

**3.5. Fitness Functions.** The fitness function is employed to determine the optimal selection of female chicks, hens, and male roosters based on chicken swam groupings. The chicken with the highest fitness grade is classified as a rooster, and each rooster is the group's leader. Chickens classified as chicks have a low fitness value, while hens have a high fitness value.

$$Qg = \frac{1}{d} \sum_{y=1}^{d} P_d - \varsigma \tag{3.14}$$

Initialization of the population lets us begin by populating the populace with D roosters, Y chicks, S hens, and Z mother hens.

**3.6. Fitness Evaluations.** It is analyzed to determine the ideal chickens, as indicated in Equation (9). We've updated the rooster's location. The roosters with the most significant fitness values receive priority over the hens with the lowest fitness values when it comes to eating. On the other hand, the chickens keep to the group's rooster in quest of food. However, they protect their food from other chickens. Birds randomly take food from other chickens. Simply put, roosters with a higher fitness value seek food in more locations than those with a lower fitness value. As a result, the corrected rooster equation 3.14 to 3.17 is as follows:

$$h^r_{x,y} = h^r_{x,y} \times \left(1 + \delta\left(0, l^2\right)\right) \tag{3.15}$$

$$h^{r+1}_{x,y} = h^r_{x,y} + h^r_{x,y} \delta\left(0, l^2\right) \tag{3.16}$$

$$h^{r+1}_{x,y} - h^r_{x,y} = h^r_{x,y} \delta\left(0, l^2\right) \tag{3.17}$$

where $\delta(0, l^2)$ specifies with the mean 0 and standard deviation $l^2$ for Gaussian distribution.

$$U^{\beta}\left[h^{r+1}_{x,y}\right] = h^r_{x,y} \delta\left(0, l^2\right) \tag{3.18}$$

$$h^{r+1}_{x,y} = h^r_{x,y}\left(\beta + \delta\left(0, l^2\right)\right) + \frac{1}{2}\beta h^{r-1}_{x,y} + \frac{1}{6}\left(1-\beta\right) h^{r-2}_{x,y} + \frac{1}{24}\beta\left(1-\beta\right)\left(2-\beta\right) h^{r-3}_{x,y} \tag{3.19}$$

In this context, let y represent the most minor constant and m be the rooster index., p is the fitness value of the associated g order between [0, 1].

$$h_{x,y} = \left\{1, _{exp\left(\frac{qm-qlxx}{qx+y}\right)}, otherwise^{if qx \leq qmim \epsilon [1,B], m \neq y}\right\} \tag{3.20}$$

The location of Hen has been changed. Hen accompanies their groupmate rooster on his food seek. By and large, the Hen snatches food that other chickens randomly discover. In comparison to submissive hens, dominant hens have an advantage. As a result, the equation for the hen update is as follows: and shown in eq 3.18 to 3.22.

$$r + 1_{x,y} = h^r_{x,y} + K1 \times l \times \left(h^r_{xm,y} - h^r_{x,y}\right) + K2 \times l \times \left(h^r_{x2,y} - h^r_{x,y}\right) \tag{3.21}$$

where the term k1 and k2 are specified as,

$$k1 = exp\left(\frac{\left(q_x - q_{h1}\right)}{bs\left(q_x\right) + y}\right) \tag{3.22}$$

$$k1 = exp\left(q_{h2} - q_x\right) \tag{3.23}$$

where k is a number between 0 and 1, the xth hen group's mate is identified by the rooster index h1. Furthermore, the variable h2 represents the chicken index of the swarm, indicating whether the individual is a hen or a rooster, so h2, h1, and hl all equal h2. Changes in chick position These dominant chicks have an advantage over other chicks regarding food completion. As a result, as illustrated in the equation below, the chicks travel about the mother looking for food.

$$h^r_{x,y} + l \times \left(h^r_{u,y} - h^r_{x,y}\right) \tag{3.24}$$

where $h_{u,y}$ is the position of the mother of the xth chick can be represented as u, where u is an element of the interval $u \in [1, A]$. The parameter L, which lies within the interval L(L [0, 2]), indicates whether the chick forages with its mother. As a result, each chick's parameter L randomly selects values between 0 and 2 h(r+1) _(x,y) shown in eq 3.23 and 3.24

**3.7. Pseudocode for Classification.**

*Algorithm – RCNN Based Brain Tumor Classification.* Input: Feature set (set of optimize feature and the area of the tumor)

Output: Decision on the tumor type

1: Initialize weight vector Q = 0;
2: Select data points in the coordinate of Bi, Ci
3: if Selected vector xi if misclassified then
4: Select Q ← B + sign(f(Bi , Ci))(Bi , Ci)
5: else
6: Repeat from step 2 until all the data are classified correctly
7: end if
8: After convergence or classification of data select Equation

**3.8. Classification Algorithms Process.** The process of the algorithm is as follows:

Step 1: Initially, Convert medical images of the brain tumor to the DICOM file format.
Step 2: Deal with medical images of a size similar to the brain. Differentiate normal from abnormal MRI pictures.
Step 3: Process the images using CSO feature extraction optimization by taking mathematical derivation using equations from 3.1 and 3.12.
Step 4: Calculate the elapsed time and use equation 3 to find the best-produced image.
Step 5: The impacted region can readily be separated by selecting the best-generated image and using the appropriate filtering algorithms.

**4. Results and Discussion.**

**4.1. Data Collection.** The collection of Dataset from the data underlying this article is available in BRATS 2015 at https://www.smir.ch/BRATS/Start2015 and https://github.com/topics/brats, respectively. Meningiomas, gliomas, and pituitary gland tumors are all in this group [23]. Rembrandt [24] includes data from 874 tumor examples from the glioma molecular diagnostic effort. This includes 566 X 566 gene expression arrays, 834 arrays of copy number data, and 13,472 points of clinical phenotype. Many deep learning-DL methods exist to find and classify brain tumors [25-28].

**4.2. Experimental Setup.** To implement the proposed methodology, we used the Google Colab environment. The following are the configuration details for the simulation trials that were used:

- Implementation environment and packages
- Google Colab
- Tensor flow
- Numpy
- Pandas, matplotlib
- Input Dataset : BRATS 2015

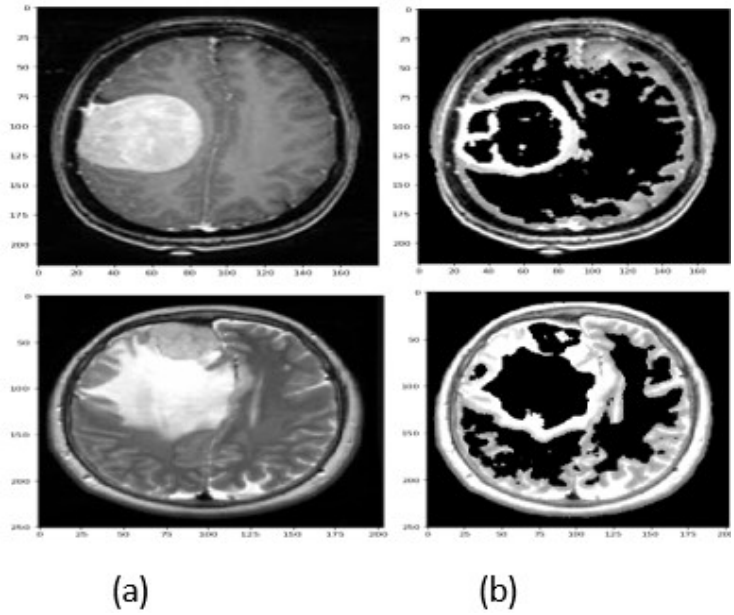


Fig. 4.1: (a) Input images (b) Optimized images

Table 5.1: Precision Analysis of RCNN technique with existing methods.

| **Method or % of training data** | **40 %** | **50 %** | **60 %** | **70 %** | **80 %** |
|---|---|---|---|---|---|
| RCNN | 91.23 | 92.42 | 93.63 | 92.38 | 92.11 |
| CNN | 90.56 | 90.89 | 91.34 | 91.63 | 91.73 |
| KSVM | 87.84 | 87.98 | 88.21 | 88.53 | 89.11 |
| SVM | 84.94 | 85.18 | 86.01 | 87.21 | 88.93 |
| RF | 83.71 | 83.95 | 85.47 | 86.76 | 87.9 |

Figure 4.1 shows the optimized brain images with clear identification of tumors. Figure 4.1(a) shows the MRI brain images with cancer, and Figure 4.1 (b) shows the optimized image after applying the CSO.

**5. Performance Validation.**

**5.1. Precision.** The precision analysis of the RCNN approach with existing techniques is shown in Table 5.1 and Figure 5.1. The results prove that the RCNN approach has improved precision with all training datasets. For example, the RCNN technique with a 40% dataset has achieved a superior precision of 91.23%, whereas the CNN, KSVM, SVM, and RF methods have achieved lesser precisions of 90.56%, 87.84%, 84.94%, and 83.71%, respectively. Similarly, using an 80% dataset, the RCNN approach achieved the highest precision of 92.11%, while the CNN, KSVM, SVM, and RF procedures achieved lower precision of 91.73%, 89.11%, 88.93%, and 87.90%, respectively.

**5.2. Sensitivity.** The sensitivity analysis of the RCNN approach with existing techniques is shown in Table 5.2 and Figure 5.2. The results prove that the RCNN approach has an improved sensitivity with all training datasets.

**5.3. Specificity.** Table 5.3 shows the Specificity of different machine learning algorithms on an image recognition task when trained on different percentages of the training data. The table shows the following: The method or percentage of training data used to train the model The Specificity of a RCNN model trained on 40

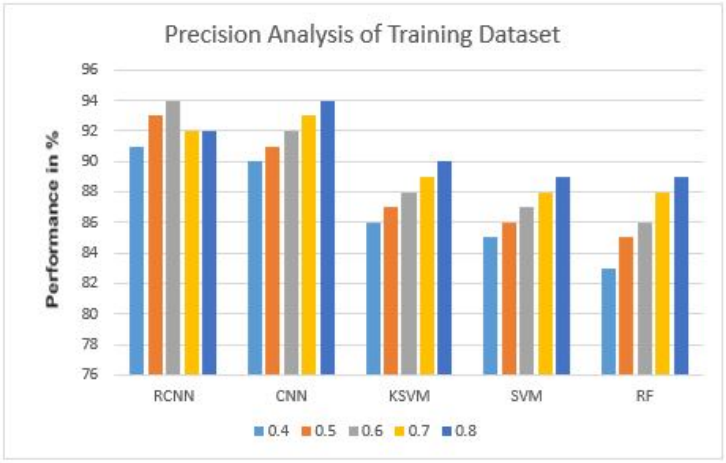


Fig. 5.1: Precision Analysis of RCNN technique with existing methods

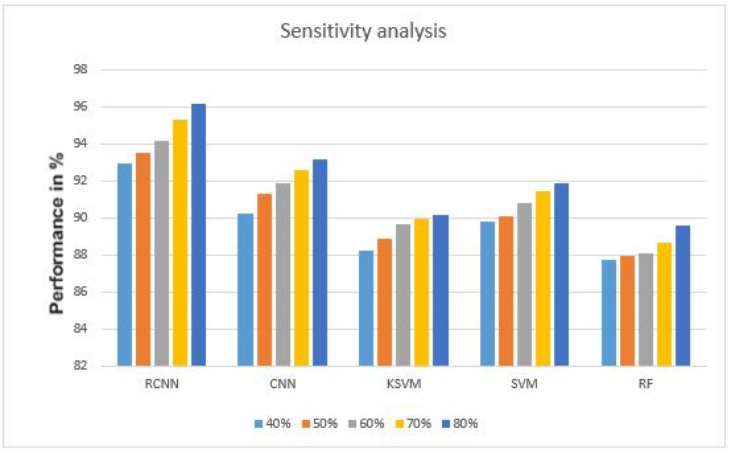


Fig. 5.2: Sensitivity Analysis of RCNN technique with other existing methods.

%, 50 %, 60 %, 70 %, and 80 % of the training data The Specificity of a CNN model trained on 40 %, 50 %, 60 %, 70 %, and 80 % of the training data The Specificity of a KSVM model trained on 40 %, 50 %, 60 %, 70 %, and 80 % of the training data The Specificity of a SVM model trained on 40 %, 50 %, 60 %, 70 %, and 80 % of the training data The Specificity of a RF model trained on 40 %, 50 %, 60 %, 70 %, and 80 % of the training data In all cases, the Specificity of the model increases as the percentage of training data used increases. This is because the model has more data to learn from, which allows it to better generalize to unseen data. The RCNN model achieves the highest Specificity overall, with a Specificity of 96.43 % when trained on 80 % of the training data. The CNN model is a close second, with a Specificity of 94.28 % when trained on 80 % of the training data. The KSVM, SVM, and RF models all have lower Specificity, but still achieve good performance. It is important to note that this table only shows the results for one image recognition task. The Specificity of these models would likely vary depending on the specific task and dataset. However, the table does illustrate the general trend that machine learning models tend to perform better when trained on more data. Here are some additional things to consider when interpreting this table: The specific image recognition task that the models were trained on is not shown in the table. This could be an important factor in how well the models perform. The size and quality of the training data is not shown in the table. These factors can also affect the

Table 5.2: Analysis of how sensitive the RCNN method is to current methods.

| Method or % of training data | 40 % | 50 % | 60 % | 70 % | 80 % |
|---|---|---|---|---|---|
| RCNN | 92.92 | 93.49 | 94.18 | 95.27 | 96.15 |
| CNN | 90.23 | 91.33 | 91.89 | 92.61 | 93.18 |
| KSVM | 88.21 | 88.89 | 89.64 | 89.95 | 90.12 |
| SVM | 89.81 | 90.11 | 90.83 | 91.41 | 91.87 |
| RF | 87.73 | 87.94 | 88.11 | 88.67 | 89.56 |

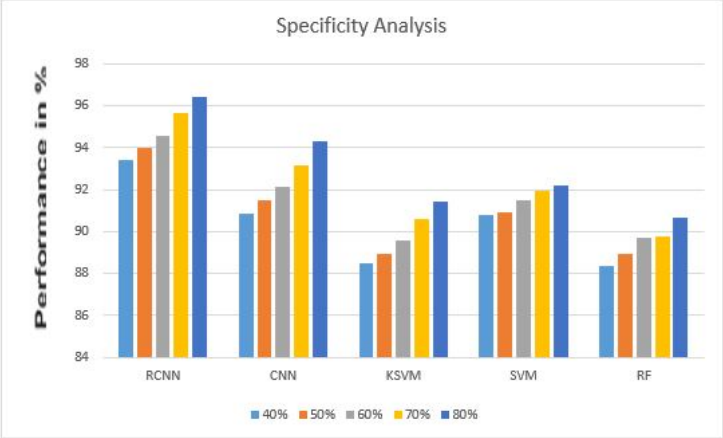


Fig. 5.3: Analysis of how sensitive the RCNN method is to current methods

performance of machine learning models. The hyper parameters of the machine learning models are not shown in the table. Hyper parameters are settings that can be tuned to improve the performance of a model.

The specificity analysis of the RCNN approach with existing techniques is shown in Table 5.3 and Figure 5.3. The results prove that the RCNN approach has an improved specificity with all training datasets.

**5.4. Accuracy.** The accuracy analysis of the RCNN approach with existing techniques is shown in Table 5.4 and Figure 5.4. The results prove that the RCNN approach has improved accuracy with all training datasets.

**5.5. Overall Accuracy Analysis.** The overall accuracy analysis of the RCNN approach with existing techniques is shown in Figure 5.5. The result depicts that the RCNN approach has improved overall accuracy with all training datasets, where the RCNN technique has achieved a superior accuracy of 95.78%, while the CNN, KSVM, SVM, and RF methods have achieved lesser accuracy of 93.23%, 92.67%, 91.14%, and 92.93%, respectively.

**5.6. TPR and FPR Analysis.** The True Positive Rate and False Positive Rate Analysis of the RCNN Method with Current Methods is shown in Figure 5.6. The results prove that the RCNN approach has an improved TPR with all training datasets. The complete analysis is shown in the table Table 5.3 and 5.4 as figure 5.6.

It is a medical image segmentation competition where researchers develop algorithms to automatically segment brain tumors from magnetic resonance imaging (MRI) scans. In the challenge, participants submit models that are evaluated on a held-out test set. The models are evaluated on how well they can segment four different regions of the brain tumor: the whole tumor (WT), the tumor core (TC), the enhancing tumor (ET), and the necrotic and non-enhancing tumor (NET). The bar graph in the image shows the average accuracy of each model across all four subregions. As you can see, the average accuracy of a model is about 95 %, while the average accuracy of another model is about 70 %. Overall, the accuracy of the models ranges from about 60

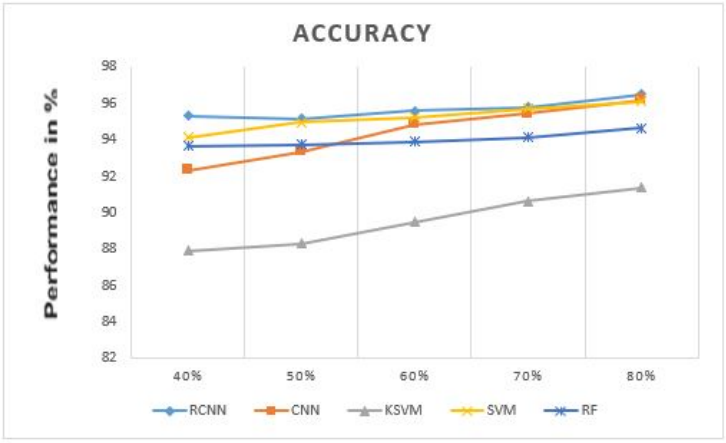


Fig. 5.4: RCNN technique's accuracy compared to current methods.

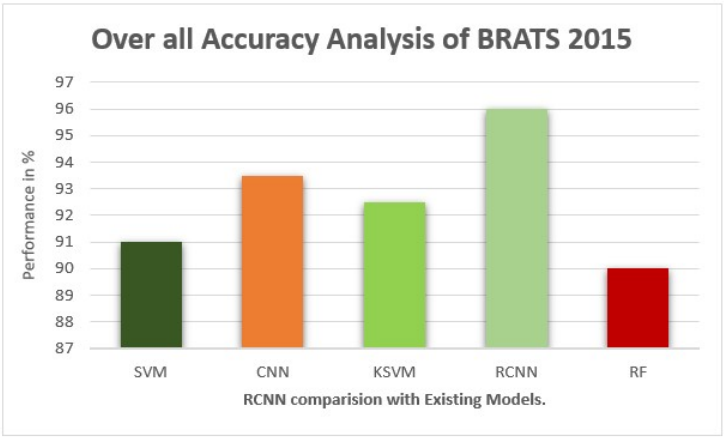


Fig. 5.5: Overall Accuracy Analysis of BRATS 2015.

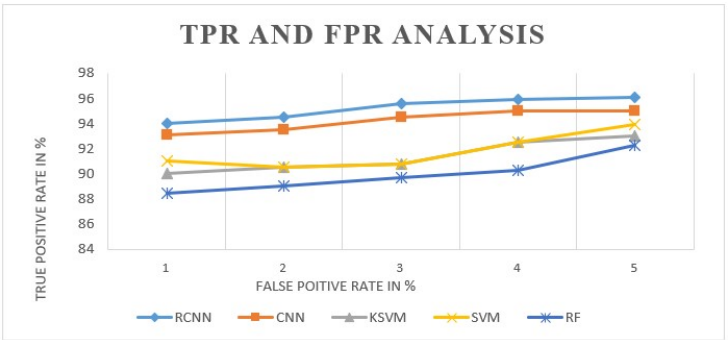


Fig. 5.6: TPR and FPR Analysis of RCNN technique with existing methods.

Table 5.3: Specificity analysis of the RCNN approach with current methods.

| **Method or % of training data** | **40 %** | **50 %** | **60 %** | **70 %** | **80 %** |
|---|---|---|---|---|---|
| RCNN | 93.42 | 93.99 | 94.58 | 95.67 | 96.43 |
| CNN | 90.83 | 91.47 | 92.14 | 93.17 | 94.28 |
| KSVM | 88.46 | 88.94 | 89.55 | 90.59 | 91.42 |
| SVM | 90.77 | 90.92 | 91.46 | 91.92 | 92.17 |
| RF | 88.34 | 88.92 | 89.71 | 89.75 | 90.68 |

Table 5.4: RCNN technique's accuracy compared to current methods.

| **Method or % of training data** | **40 %** | **50 %** | **60 %** | **70 %** | **80 %** |
|---|---|---|---|---|---|
| RCNN | 95.29 | 92.33 | 87.91 | 94.13 | 93.66 |
| CNN | 95.14 | 93.33 | 88.31 | 94.96 | 93.75 |
| KSVM | 95.58 | 94.82 | 89.47 | 95.21 | 93.9 |
| SVM | 95.77 | 95.41 | 90.63 | 95.71 | 94.14 |
| RF | 96.49 | 96.19 | 91.36 | 96.1 | 94.62 |

% to 97 %. Here are some additional things to consider when interpreting this bar graph: The specific models being compared are not shown in the image. The BRATS challenge is a competition, so the models shown in the graph are likely to be state-of-the-art models. However, it is important to remember that machine learning is an active area of research, and new models are being developed all the time shown in figure 5.4. The accuracy of a brain tumor segmentation model is just one measure of its performance. Other important factors include the sensitivity and specificity of the model. Sensitivity is the ability of the model to correctly identify people who have a brain tumor. Specificity is the ability of the model to correctly identify people who do not have a brain tumor shown in figure 5.5 and figure 5.6.

**6. Conclusion.** The proposed RCNN-CSO approach is an effective and automated way of classifying and segmenting brain tumors. The MRI pictures are enhanced by applying the Adaptive Fuzzy Filtering (AFF) approach. MRI images are segmented using a technique called chicken swarm optimization (CSO), which uses Tsallis uses entropy-based picture segments to find the damaged parts of the brain. The goal here is to examine the RCNN method, which boasts better results. A thorough experimental analysis is performed, and Several ways are used to look at the information. The overall accuracy of the RCNN technique compared to the other methods is 95.78%. The simulation results demonstrated that the suggested RCNN strategy outperformed the existing methods. The presented approaches in this paper can be used in the future to examine the influence of strokes caused by tumors on brain imaging.

REFERENCES

[1] Waktola, S., Bieberle, A., Barthel, F., Bieberle, M., Hampel, U., Grudzień, K., & Babout, L. (2018) , *A new data-processing approach to study particle motion using ultrafast X-ray tomography scanner: case study of gravitational mass flow.* Experiments in Fluids, 59, 1-14.

[2] Vasantharaj, A., Rani, P. S., Huque, S., Raghuram, K. S., Ganeshkumar, R., & Shafi, S. N. (2023), *Automated brain imaging diagnosis and classification model using rat swarm optimization with deep learning based capsule network.* International Journal of Image and Graphics, 23(03), 2240001.

[3] Meng, X., Liu, Y., Gao, X., & Zhang, H. (2014), *A new bio-inspired algorithm: chicken swarm optimization.* In Advances in Swarm Intelligence: 5th International Conference, ICSI 2014, Hefei, China, October 17-20, 2014, Proceedings, Part I 5 (pp. 86-94). Springer International Publishing.

[4] Shivaprasad, B. J., Ravikumar, M., & Guru, D. S. (2022), *Analysis of Brain Tumor Using MR Images: A Brief Survey.* International Journal of Image and Graphics, 22(02), 2250023.

[5] Demirhan, A., Törü, M., & Güler, I. (2014) , *Segmentation of tumor and edema along with healthy tissues of brain using wavelets and neural networks.* IEEE journal of biomedical and health informatics, 19(4), 1451-1458.

[6] Srinivas, B., & Rao, G. S. (2018, January), *Unsupervised learning algorithms for MRI brain tumor segmentation.* In 2018 Conference on Signal Processing And Communication Engineering Systems (SPACES) (pp. 181-184). IEEE.

[7] Bal, A., Banerjee, M., Chakrabarti, A., & Sharma, P. (2022), *MRI brain tumor segmentation and analysis using rough-fuzzy c-means and shape based properties.* Journal of King Saud University-Computer and Information Sciences, 34(2), 115-133.

[8] Manocha, P., Bhasme, S., Gupta, T., Panigrahi, B. K., & Gandhi, T. K. (2017), *Automated tumor segmentation and brain mapping for the tumor area.* arXiv preprint arXiv:1710.11121.

[9] Varuna Shree, N., & Kumar, T. N. R. (2018) , *Identification and classification of brain tumor MRI images with feature extraction using DWT and probabilistic neural network.* Brain informatics, 5(1), 23-30.

[10] Tomicka, J., Cichoń, K., Chlewicki, W., Holicki, M., Pelc, M., Zygarlicki, J., Podpora, M. & Kawala-Sterniuk, A., 2022 , *Pilot Study on Application for Analysis of Magnetic Resonance Spectroscopy Spectra.* IFAC-PapersOnLine, 55(4), pp.45-50.

[11] Kumar, S., & Mankame, D. P. (2020) , *Optimization driven deep convolution neural network for brain tumor classification.* Biocybernetics and Biomedical Engineering, 40(3), 1190-1204.

[12] D. Rammurthy, & P.K. Mahesh, 2022. , *Whale Harris Hawks Optimization based deep learning classifier for brain tumor detection using MRI images.* Journal of King Saud University – Computer and Information Sciences, 34, 3259-3272

[13] D. Deb & S. Roy, 2021 , *Brain tumor detection based on hybrid deep neural network in MRI by adaptive squirrel search optimization, Multimed.* Tools. 80 (2) 2621–2645.

[14] Yin, B., Wang, C., & Abza, F. (2020) , *New brain tumor classification method based on an improved version of whale optimization algorithm.* Biomedical Signal Processing and Control, 56, 101728.

[15] Sultan, H. H., Salem, N. M., & Al-Atabany, W. (2019), *Multi-classification of brain tumor images using deep neural network.* IEEE access, 7, 69215-69225.

[16] Pandiselvi, T., & Maheswaran, R. (2019) , *Efficient framework for identifying, locating, detecting and classifying MRI brain tumor in MRI images.* Journal of medical systems, 43, 1-14.

[17] Deepak, S., & Ameer, P. M. (2021) , *Automated categorization of brain tumor from mri using cnn features and svm.* Journal of Ambient Intelligence and Humanized Computing, 12, 8357-8369.

[18] Narmatha, C., Eljack, S. M., Tuka, A. A. R. M., Manimurugan, S., & Mustafa, M. (2020) , *A hybrid fuzzy brain-storm optimization algorithm for the classification of brain tumor MRI images.* Journal of ambient intelligence and humanized computing, 1-9.

[19] Polepaka, S., Rao, C. S., & Chandra Mohan, M. (2020) , *IDSS-based two stage classification of brain tumor using SVM.* Health and Technology, 10(1), 249-258.

[20] Menze, B. H., Jakab, A., Bauer, S., Kalpathy-Cramer, J., Farahani, K., Kirby, J., ... & Van Leemput, K. (2014) , *The multimodal brain tumor image segmentation benchmark (BRATS).* IEEE transactions on medical imaging, 34(10), 1993-2024.

[21] Cristin, D. R., Kumar, D. K. S., & Anbhazhagan, D. P. (2021) , *Severity level classification of brain Tumor based on MRI images using fractional-chicken swarm optimization algorithm.* The Computer Journal, 64(10), 1514-1530.

[22] Paul, J. S., Plassard, A. J., Landman, B. A., & Fabbri, D. (2017, March), *Deep learning for brain tumor classification.* In Medical Imaging 2017: Biomedical Applications in Molecular, Structural, and Functional Imaging (Vol. 10137, pp. 253-268). SPIE.

[23] Cheng, J., Huang, W., Cao, S., Yang, R., Yang, W., Yun, Z., ... & Feng, Q. (2015) , *Enhanced performance of brain tumor classification via tumor region augmentation and partition.* PloS one, 10(10), e0140381.

[24] Sayah, A., Bencheqroun, C., Bhuvaneshwar, K., Belouali, A., Bakas, S., Sako, C., ... & Gusev, Y. (2022). , *Enhancing the REMBRANDT MRI collection with expert segmentation labels and quantitative radiomic features.* Scientific Data, 9(1), 338.

[25] Noreen, N., Palaniappan, S., Qayyum, A., Ahmad, I., Imran, M., & Shoaib, M. (2020) , *A deep learning model based on concatenation approach for the diagnosis of brain tumor.* IEEE Access, 8, 55135-55144.

*Edited by:* Polinpapilinho F. Katina
*Special issue on:* Scalable Computing in Online and Blended Learning Environments: Challenges and Solutions
*Received:* Jan 7, 2024
*Accepted:* Mar 23, 2024